Modeling and Numerical Simulation of Material Science, 2025, 15(1), 1-15
https://www.scirp.org/journal/mnsms
ISSN Online: 2164-5353
ISSN Print: 2164-5345

Numerical Simulation and Analysis of Heat Treatment Processes on AISI 1025 Steel Produced by Laser Engineered Net Shaping

Elphas Tum[1,2,3,4*], Rehema Ndeda[1], James Mutua[5], Raghupatruni Prasad[3,4,6], Eyitao Olakanmi[2,3,4], Sisa Pityana[7]

[1]Department of Mechatronic Engineering, Jomo Kenyatta University of Agriculture and Technology, Juja, Kenya
[2]Department of Mechanical, Energy and Industrial Engineering, Botswana International University of Science and Technology, Palapye, Botswana
[3]Advanced Manufacturing and Engineering Education (AMEE) Research Group, Botswana International University of Science and Technology, Palapye, Botswana
[4]UNESCO Chair on Sustainable Manufacturing and Innovation Technologies (UCoSMIT) Team, Botswana International University of Science and Technology, Palapye, Botswana
[5]Department of Mechanical Engineering, Jomo Kenyatta University of Agriculture and Technology, Juja, Kenya
[6]Department of Chemical, Materials and Metallurgical Engineering, Botswana International University of Science and Technology, Palapye, Botswana
[7]National Laser Centre, Council for Scientific and Industrial Research, Pretoria, South Africa
Email: *tumkibet@gmail.com

How to cite this paper: Tum, E., Ndeda, R., Mutua, J., Prasad, R., Olakanmi, E. and Pityana, S. (2025) Numerical Simulation and Analysis of Heat Treatment Processes on AISI 1025 Steel Produced by Laser Engineered Net Shaping. *Modeling and Numerical Simulation of Material Science*, **15**, 1-15.
https://doi.org/10.4236/mnsms.2025.151001

Received: October 2, 2024
Accepted: November 11, 2024
Published: November 14, 2024

Abstract

Heat treatment processes, such as annealing and quenching, are crucial in determining residual stress evolution, microstructural changes and mechanical properties of metallic materials, with residual stresses playing a greater role in the performance of components. This paper investigates the effect of heat treatment on residual stresses induced in AISI 1025, manufactured using LENS. Finite element model was developed and simulated to analyze residual stress development. AISI 1025 samples suitable for tool and die applications in Fused Deposition Modelling (FDM) filament production, were fabricated using Laser Engineered Net Shaping (LENS) process, followed by heat treatment where annealing and quenching processes were done. The material's microstructure, residual stress and hardness of heat-treated samples under investigation, were compared against the as-built samples. The results indicated that after annealing, tensile residual stresses were reduced by 93%, resulting in a reduced crack growth rate, compared to the as-built sample, although the hardness was reduced significantly by 25%. On the other hand, high tensile residual stresses of 425 ± 14 MPa were recorded after quenching process with an improvement of hardness by 21%.

Keywords

Heat Treatment, Residual Stresses, Hardness, Microstructure, Numerical Simulation

1. Introduction

1.1. Laser Engineered Net Shaping Process

Laser Engineered Net Shaping (LENS) is an Additive Manufacturing (AM) process that utilizes laser energy to melt powder or wire material in the deposition of components. LENS technique can produce intricate parts, reduce material waste and improve mechanical properties compared to certain traditional methods [1]. Although LENS process has several advantages, residual stresses still remain a great challenge during the deposition process. Residual stresses arise due to non-uniform thermal gradients, phase transformations, and plastic deformation during heating and cooling [2]. Residual stress in metal components can cause the material to be pulled, pushed, or deformed, depending on its direction [3]. Consequently, additive-manufactured metal parts are prone to distortion, cracking, and reduced fatigue strength when residual stress is present. The structural dependability under cyclic loads negatively impacts the component's performance due to residual stress. Understanding and controlling these residual stresses is crucial for optimizing the mechanical performance of deposited parts especially for critical applications such as tool and dies used for plastic filament production that require optimal performance. Previous studies have applied substrate preheating [4] optimization of laser parameters [5] and stress relief heat treatment [6] as a way to remedy residual stress development. This highlights the potential for utilizing heat treatment to achieve desired material properties.

1.2. Heat Treatment Processes

Heat treatment processes are popular in the manufacturing industry in enhancing mechanical properties of materials. Annealing process is mostly used as a stress relief method, where it involves heating the material to a specific temperature and then cooling it slowly. The reduction of residual stress increases the toughness of a part by removing high tensile stresses at the surface [7]. Quenching, on the other hand, involves rapid cooling, usually in water or oil, to increase hardness and strength by forming martensitic structures [8]. Both experimental and numerical methods have been used to evaluate the impact of heat treatment on different materials [9]-[11]. Numerical simulation is commonly used to understand how a process operates virtually through replicating the actual parameters in experimental scenario [11], and thus can be used in optimizing properties of a component. Finite element method provides a powerful approach to predicting and analyzing residual stresses due to its accuracy and ability to replicate the real process [12]. Studies have been carried out to develop numerical models that simulate

residual stresses in the LENS process [13] and heat treatment methods targeting residual stress relaxation [14]. The simulation of residual stresses developed during LENS deposition and heat treatment processes comprises both thermal and mechanical analysis. Thermal analysis calculates the temperature distribution, while mechanical analysis assesses the residual stresses caused by thermal loads.

Experimental methods have been previously used to measure residual stresses [15]. However, recent advancements have led to adoption of numerical approaches due to their flexibility and cost-effectiveness. For instance, De Baere *et al.* [11] employed Abaqus CAE to model the stress relief heat treatment process, effectively simulating the complex interactions between temperature and stress development. The accuracy of such models depends on correct implementation of thermal and mechanical properties, including temperature-dependent material behavior, phase transformations, and plasticity effects. This highlights the need for well-developed numerical model to ensure reliable predictions.

1.3. AISI 1025 Alloy

AISI 1025 steel is an important industrial consideration due to its balanced mechanical performance and cost, with a carbon content ranging from 0.22% to 0.28%, manganese (0.60% - 0.90%) and trace amounts of phosphorus and sulfur. The alloy gives a balance between strength, ductility, and toughness, thus enabling its usage in applications requiring moderate mechanical properties such as in automotive, tool and die, construction, machinery industries. In filament die manufacturing, particularly for Fused Deposition Modeling (FDM), AISI 1025 is a valuable material due to its cost effectiveness, good wear resistance, machinability, and moderate mechanical properties. However, the main challenge in production process is managing residual stress and ensuring optimal material hardness. Residual stresses that occur during the manufacturing process, can cause dimensional inaccuracies and reduce the lifespan of dies by inducing cracks under cyclic thermal loads. Therefore, reduction of residual stresses and improvement of hardness for AISI 1025 is essential in optimizing die performance.

Low-carbon steels such as AISI 1025 alloy can be manufactured using several methods such as, casting, forging, and additive manufacturing (AM). Although these processes are prone to residual stress formation, heat treatment processes such as annealing can be used in reducing these stresses and thus can aid in tailoring the material properties of AISI 1025 to meet specific application requirements. Studies on additive manufacturing of low carbon steel have shown the possibility of producing AISI 1025 alloy steel, for instance, Rafieazad *et al.* [16] explored the AM process for low-carbon steels, focusing on microstructural development and mechanical properties. Another study by Chae *et al.* [17] investigated the challenges of residual stress in AM-produced low-carbon steels, examining strategies for mitigating these stresses through post-processing heat treatments. These studies highlight the potential of AM in producing AISI 1025 components, since specific studies on additive manufacturing of AISI 1025 are still limited. This paper aims to fill this gap by providing an investigation of numerical and

experimental study of the impact of heat treatment on residual stress development in AMed AISI 1025, along with understanding the resulting microstructural changes, and mechanical properties.

2. Methodology

2.1. Material Selection

The material used for this study was AISI 1025 steel, known for its applications in mechanical components such as drive shafts, construction materials, and tools and dies. An XRF analysis of the chemical composition of AISI 1025 is shown in Table 1. The material properties such as density, Poisson's ratio, tensile strength and resistivity are illustrated in Table 2. The temperature dependent thermal properties, including thermal conductivity and specific heat, are illustrated in Figure 1.

Table 1. Chemical composition of AISI 1025 from XRF analysis (wt%).

C	Mn	S	Si	Cr	Fe
0.22	0.35	0.316	0.781	0.202	Bal

Table 2. Material properties of AISI 1025.

Material Property	Value
Density	7858 kg/m^3
Coefficient of Thermal Expansion	1.2e−005˚C
Specific Heat	486 J/kg˚C (0 - 100˚C)
Thermal Conductivity	51.9 W/m/˚C (0 - 100˚C)
Resistivity	1.7e−04-ohm mm
Tensile/Compressive Yield Strength	370 MPa
Tensile Ultimate Strength	440 Mpa

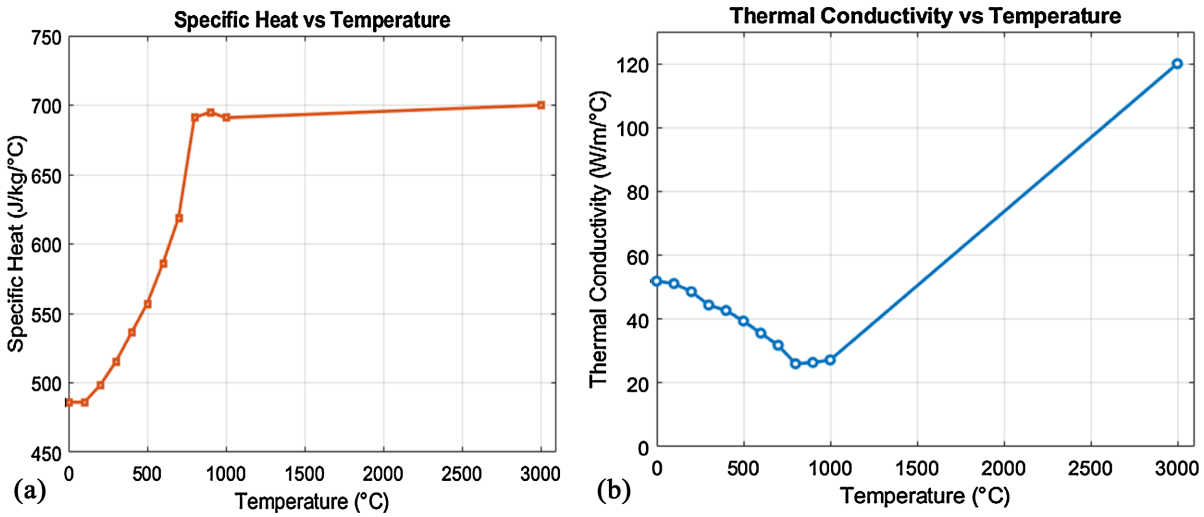

Figure 1. Temperature dependent material properties of AISI 1025.

2.2. Finite Element Model

A 3D model, cylindrical in shape of 12.7 mm by 5 mm on a substrate measuring 50 mm by 50 mm by 10 mm, was created in ANSYS Workbench 2024 software. The dimensions were chosen to reflect a typical industrial application, ensuring that the model captures the critical aspects of heat transfer and stress development during heat treatment. A fine mesh was used (**Figure 1(b)**) after a convergence study as shown in **Figure 2(a)**, to ensure reliability of the model in capturing the steep temperature gradients and stress concentrations. The model was validated with the results from a study by Kik *et al.* [18], demonstrating the model's capability to predict heat treatment outcomes.

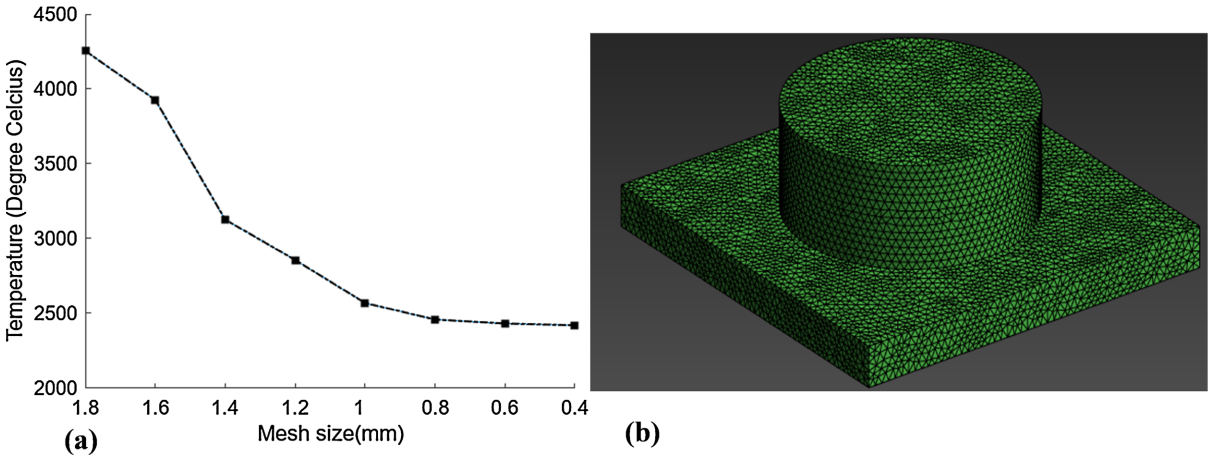

Figure 2. (a) Mesh sensitivity analysis; (b) Finite element meshing.

The thermal analysis was employed to simulate the temperature distribution during heating and cooling, followed by a structural analysis to compute the resulting residual stresses. The coupled thermal-mechanical analysis allows for an understanding of the interaction between temperature changes and stress development.

2.3. Governing Equations and Boundary Conditions

The temperature of 850˚C was applied as the maximum heating temperature for the sample to illustrate the heating temperature used in the real furnace. The ambient temperature of was assumed to be 40˚C which was selected to be the lowest temperature of cooling. The basic heat transfer law of temperature field according to Fourier's law. The three-dimensional heat transfer differential equation also known as conservation law of energy is expressed as shown in Equation 1 [19].

$$\rho c_p \frac{\partial T}{\partial \tau} = \lambda \frac{\partial^2 T}{\partial x_i^2} + \sigma_{ij} \dot{\varepsilon}_{ij}^p - \sum \rho_I l_I \dot{\zeta}_I, \tag{1}$$

where, T is the temperature [K], l_I is the latent heat due to phase transformation [J/Kg], λ—heat conductivity coefficient [W·m^{-1}·K^{-1}], C_p—specific heat [J·kg^{-1}·K^{-1}], and ρ—mass density [kg·m^{-3}]. Phase transformation during quenching were

modeled using the Johnson-Mehl-Avrami-Kolmogorov (JMAK) equation [20], which describes the kinetics of austenite-to-martensite transformation [20]. The transformed volume fraction on time f_V, was calculated by Equation (2).

$$f_V = 1 - \exp\left(-kt^n\right) \tag{2}$$

where k is temperature dependent rate and n is the Avrami exponent. The thermal convection and radiation were taken into account as per Newton's law of cooling and Stefan-Boltzmann law respectively, as shown in Equations (3) and (4) [21].

$$q_c = Ah\left(T - T_a\right) \tag{3}$$

$$q_r = \epsilon_r \sigma_r \left(T^4 - T_a^4\right) \tag{4}$$

where q_c represents heat transferred through convection and q_r heat transfer through radiation. The variable h represents the heat transfer coefficient associated with natural thermal convection, while A denotes the heat transfer area. The value of σ_r corresponds to the Stefan-Boltzmann constant, set at 5.67e−8 W/m·K. Lastly, the variable ϵ_r represents the coefficient of radiation emissivity for the material.

In thermal treatment simulations, plastic flow stress (σ) calculations depend on the flow stress curve of each phase, and can be defined in terms of strain (ε), temperature (T) and strain rate ($\dot{\varepsilon}$) [22], as illustrated in Equation 5. Whereas the total strain rate is defined by Equation (6).

$$\overline{\sigma} = \overline{\sigma}\left(\varepsilon, \dot{\varepsilon}, T\right) \tag{5}$$

$$\dot{\varepsilon}_{ij} = \dot{\varepsilon}_{ij}^t + \dot{\varepsilon}_{ij}^e + \dot{\varepsilon}_{ij}^p + \dot{\varepsilon}_{ij}^{tr} + \dot{\varepsilon}_{ij}^{tp} \tag{6}$$

where $\dot{\varepsilon}_{ij}^t, \dot{\varepsilon}_{ij}^e, \dot{\varepsilon}_{ij}^p, \dot{\varepsilon}_{ij}^{tr}, \dot{\varepsilon}_{ij}^{tp}$ are the thermal, elastic, plastic, phase transformation and phase transformation plasticity strain rates.

Temperature variation during simulation was conducted according to AMS2759/4 for both annealing and quenching. For annealing, an AISI 1025 sample was subjected to a heating rate of 5˚C/min to a temperature of 850˚C, above the austenitizing temperature. The temperature was then held constant for 2 hours and then cooled down at a rate of 3˚C /min to the ambient temperature [18]. For quenching, the samples were heated the same as annealing, however the cooling rate was rapid at a rate of 99˚C/sec.

2.4. Experimental Study

A laser system, LENS 850R by Optomec was used for the deposition of samples. A laser power of 270 W, a scan speed of 7.1 mm/s, feed rate of 1.7 g/min and hatch spacing of 0.67 mm were used during the deposition. A total of 18 samples were produced at a laser spot size of 1.4 mm. Heat-treatment experiments were performed in a muffle furnace supplied by Ultra Furn. The samples were subjected to annealing and hardening, as given in the AMS2759/4 standard [23]. All the samples were placed inside the furnace at heating rate of 5˚C/min until a temperature of 850˚C was attained which is above an austenitizing temperature with a soaking

time of 2 hours. The annealing samples were then furnace cooled to ambient temperature whereas the samples for quenching were fast cooled via a water bath. The sample were then prepared for characterization as per ASTM E3-11 standard.

Samples for residual stress analysis were prepared through electrochemical etching using Pulstec electro-etching machine to achieve smooth surface finish. Whereas samples for hardness testing and microstructural investigation were initially sectioned using Struers Labotom machine available at CSIR, South Africa, the sectioned samples were subsequently mounted using an Automatic Mounting Machine, a series of grinding and polishing operations using Struers TegraPol-25 machine, were followed to ensure optimal surface quality for analysis according to ASTM E3 standard.

2.5. Characterization of Samples

Residual stress measurements were conducted prior to heat treatment in comparison with post-heat treatment results. After sample preparations, the specimens were subjected to hardness test, microstructural and phase analysis as well as residual stresses to ascertain the effects of heat treatment on mechanical properties. Phase analysis on samples was performed using a Bruker D8 powder diffractometer that utilizes X-ray diffraction (XRD). X-ray radiation with a wavelength of 1.54056 A was used, covering a scanning range of 20 to 110 degrees (2θ). The measurement of residual stress was achieved using a XRD μ-x360 Pulstec residual stress analyzer for the heat treated and as built samples as illustrated in **Figure 3(a)**. The measurements involved employing cos α technique to calculate both in-plane residual stress (σx) and shear residual stress (τxy) on a LENS produced sample illustrated in **Figure 3(b)**. Vicker's hardness testing machine of model Zwick/Roell ZHVm, was used for measuring hardness on both the as built and heat-treated samples. A load of 500 gf for 10 s was applied as per ASTM E92 standard. Microstructural analysis was achieved using Scanning Electron Microscope (SEM), JEOL JSM-6010PLUS/LA after the polished samples were etched using a 2% nital solution as per ASTM E407.

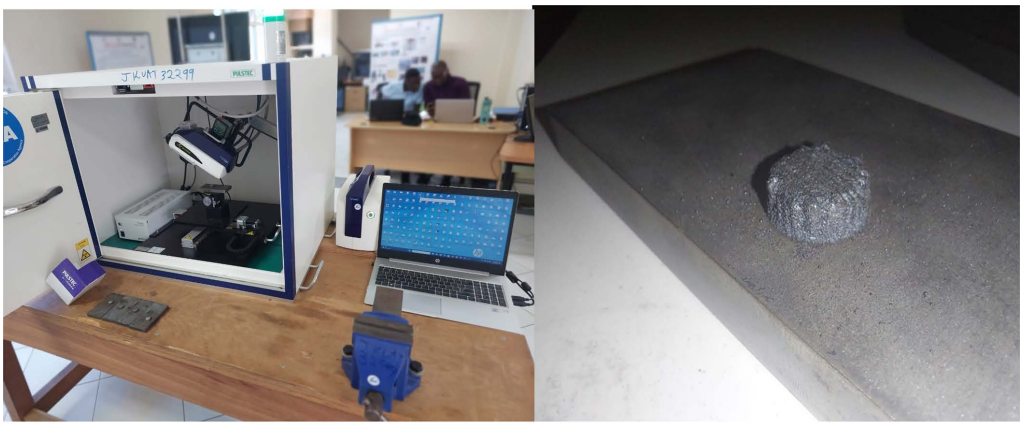

(a) (b)

Figure 3. (a) μ-x 360 Pulstec residual stress analyzer; (b) Prepared Sample in residual stress analyzer.

3. Results and Discussion

3.1. Temperature Distribution and Residual Stress Analysis

Figure 4 shows the annealing heat treatment simulations during heating, holding and cooling stages. During the heating phase the sample is subjected to elevated temperature over a specified time as is shown in Figure 4(a), this indicates that the sample has been uniformly heated to 850˚C, to reach a thermal state crucial for subsequent holding stage. The heating stage tends to reduce the thermal gradient which results in minimum stress development. During the holding stage Figure 4(b), the temperature stabilizes within (330˚C - 540˚C), allowing the material's structure to rearrange thus aids in prevention of new thermal stresses. In the cooling stage Figure 4(c), the temperature decreases gradually (22 - 125˚C). The slow cooling process is essential for preventing the development of thermal gradients that could otherwise induce high residual stresses, as seen in quenching process. The gentle cooling allows the material to contract uniformly, leading to a stress-free state. Overall, the annealing process successfully minimizes residual stresses by controlling the temperature distribution throughout all stages, resulting in a more stable material with enhanced mechanical properties and improved resistance to future stress and fatigue. Tooten *et al.* [15] highlighted that cooling phases plays a critical role in determining both magnitude and distribution of residual stresses.

Figure 5 illustrates simulation of quenching process at various stages of cooling after the heating phase. During heating (Figure 5(a)), the samples reach a peak temperature of 850˚C. When the samples were subjected to cooling, just after 2 seconds as illustrated in Figure 5(b), the temperature dropped significantly to 645˚C, within the next 15 seconds (Figure 5(c)) and 38 seconds (Figure 5(d)), the

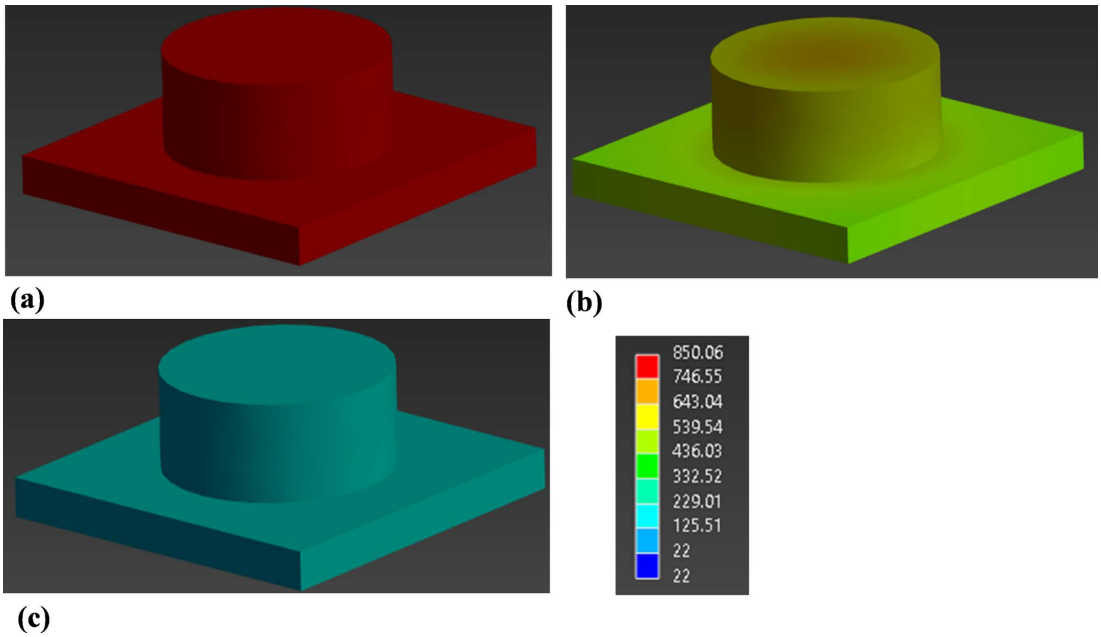

Figure 4. Simulation of annealing during three stages (a) heating; (b) holding; (c) cooling.

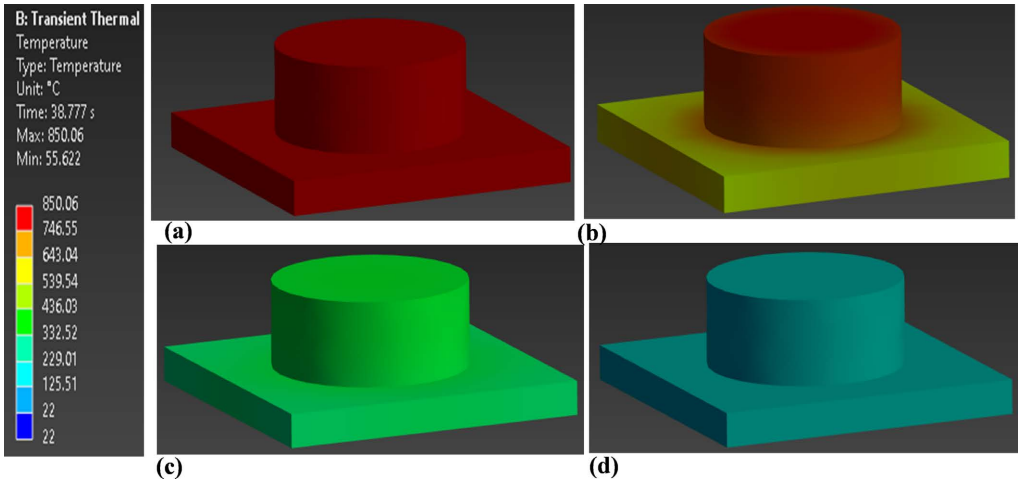

Figure 5. Simulation of quenching process during heating and cooling (a) Heating stage; (b) Cooling at 2 secs; (c) Cooling at 15 secs; (d) Cooling at 38 secs.

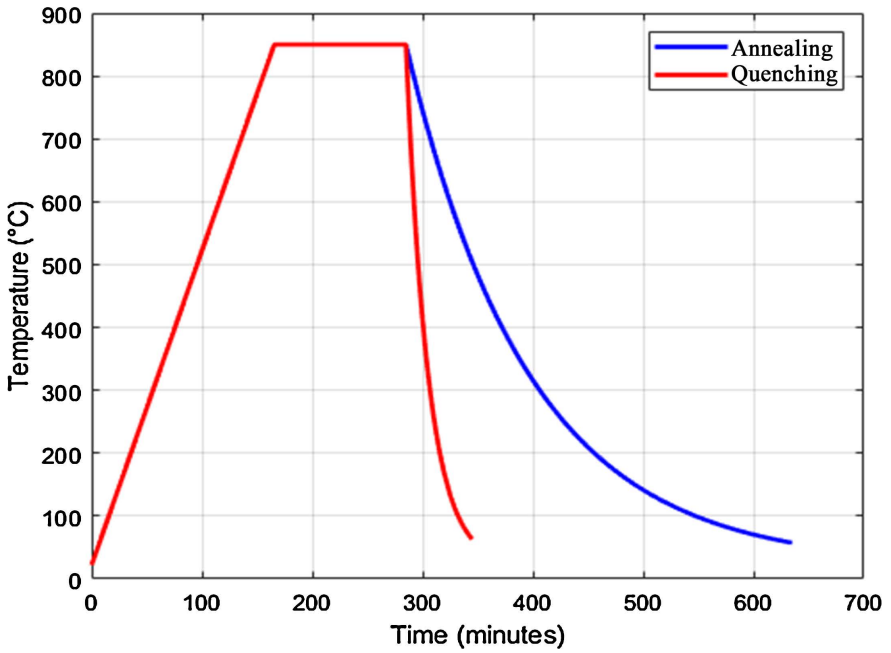

Figure 6. Temperature profile for annealing and quenching.

temperatures dropped further to 330˚C and 125˚C respectively before cooling down to room temperature. As demonstrated in **Figure 6**, the cooling rate for both annealing and quenching plays a crucial role in the formation of residual stresses. Specifically, the annealing process, which involves a slower cooling rate, leads to lower residual stresses compared to the quenching process, which features rapid cooling. The annealing sample shown in **Figure 7(a)** supports this, displaying considerably lower residual stresses with a maximum value of 34.72 Mpa. This finding is consistent with the study by Lu *et al.* [24], which indicated that slower cooling reduces residual stress and strain. Annealing involves slow cooling rates, contributing to a uniform thermal contraction that results in low magnitudes of

residual stresses. The distribution appears uniform compared to the quenched sample, with stress values nearing zero as portrayed by the contour map. This uniform distribution demonstrates that annealing effectively alleviates residual stresses, thus reducing the likelihood of material failure due to cracking.

Figure 7(b) shows residual stress distribution of a quenched sample, a significant high residual stress of 407 Mpa is observed mostly near the edges of the deposited part, this is as a result of rapid cooling process, which induces steep temperature gradients that contributes to uneven contraction within the material leading to tensile stresses at the edges and compressive stresses at the center, which can lead to cracking if not properly managed [25]. Similar patterns of residual stress distribution have been observed in [10].

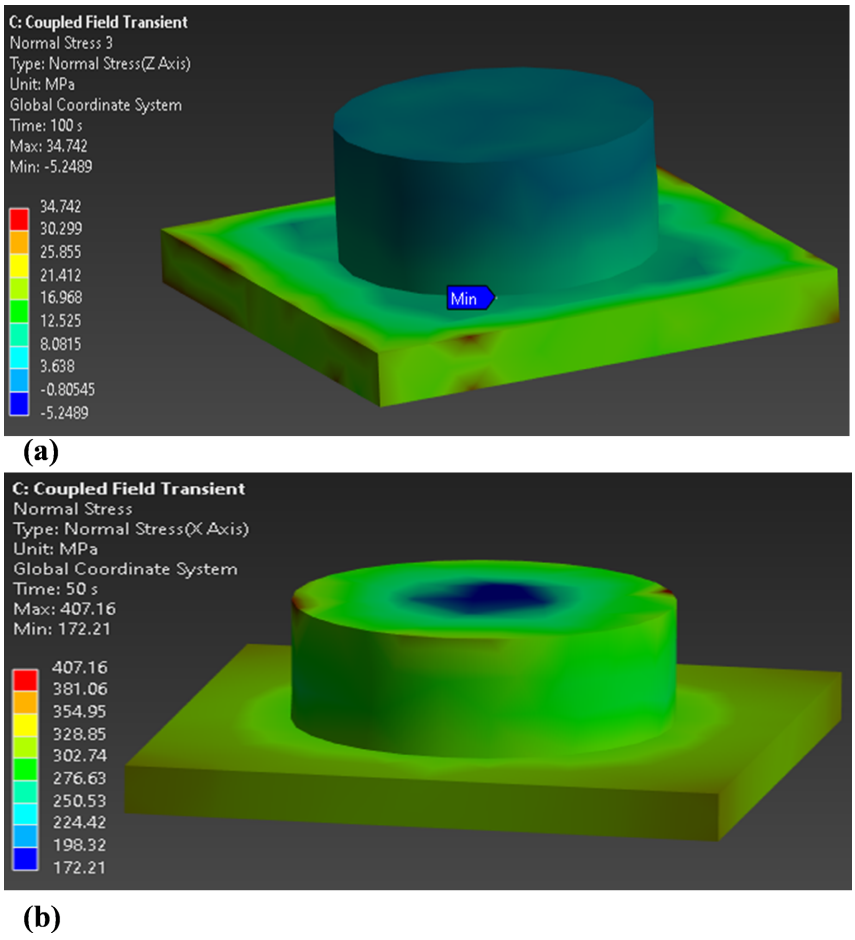

Figure 7. Residual stress distribution (a) Quenching; (b) Annealing.

3.2. Validation of Numerical Model

The numerical results were validated against experimental data. Figure 8 compares residual stresses under varying heat treatment conditions both experimental and simulation. As per experimental results, the as built and annealing samples exhibited residual stress of 144 ± 20 Mpa and −3 ± 16 MPa respectively. However, the quenching process resulted in an increase in residual stress of 425 ± 14 MPa.

These observations indicate that residual stresses in LENS fabricated AISI 1025 can be decreased by annealing, tensile stresses reduced into compressive stresses. The reduction of tensile stresses into compressive stresses is beneficial, as compressive stresses can enhance fatigue resistance and prevent crack initiation, improving the overall structural property of the material. The close agreement between the numerical and experimental results further validates the ANSYS model's capability, with minimal error of 4.24% observed between the two sets of data, confirming its reliability for simulating residual stresses in AISI 1025 steel.

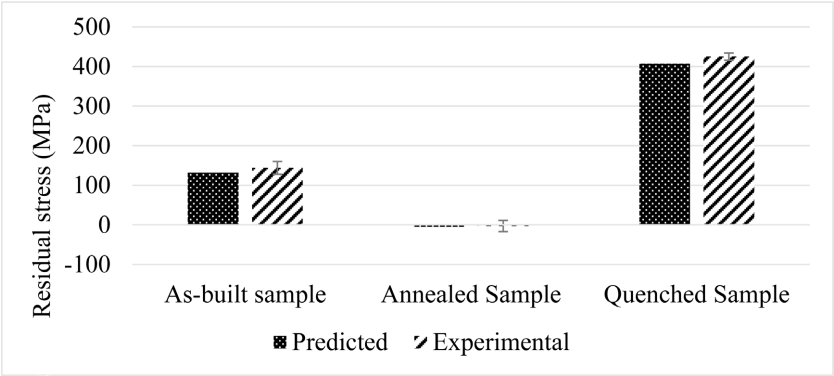

Figure 8. Effect of heat treatment on residual stress.

3.3. Microstructural and Hardness Study

The evaluation of the microstructure further explains the behaviour of AISI 1025 during heat treatment. **Figure 9** shows SEM micrographs for as-built and heat treated AISI 1025 samples. The annealed sample in **Figure 9(b)** indicates enlarged grains consisting mainly of ferrite as the main phase as illustrated in **Figure 10**. The evenly distributed homogenized grains can be attributed to the slow cooling which causes transformation of austenite to soft pearlite, displayed by the laminar structure. Coarser grains are mostly associated with improved ductility and toughness as was demonstrated by Hang *et al.* [26]. Additionally, the grain structure contributes to low residual stress magnitudes as observed with the annealing simulation. However, the hardness is reduced considerably to 126 ± 4 HV, compared to 169.17 ± HV recorded on the as built sample. The reduced hardness can be attributed to slow rate of cooling which refines previously formed grains. This agrees with Rahman *et al.* [27] who reported that annealing enhances the ductility of a material at the expense of hardness and removes internal stresses. **Figure 9(c)** illustrates a microstructure from the quenched sample, a fine highly strained grain structure is observed indicating that the grains had limited time to undergo growth due to the rapid cooling rate which contributed to high residual stresses as was depicted by the simulation.

The quenched microstructure further consists of a tempered martensite with retained austenite structure as displayed in XRD results in **Figure 11**. The rapid cooling rate prevents the complete conversion of austenite into ferrite structure; thus, the residual austenitic structure subsequently undergoes a transformation

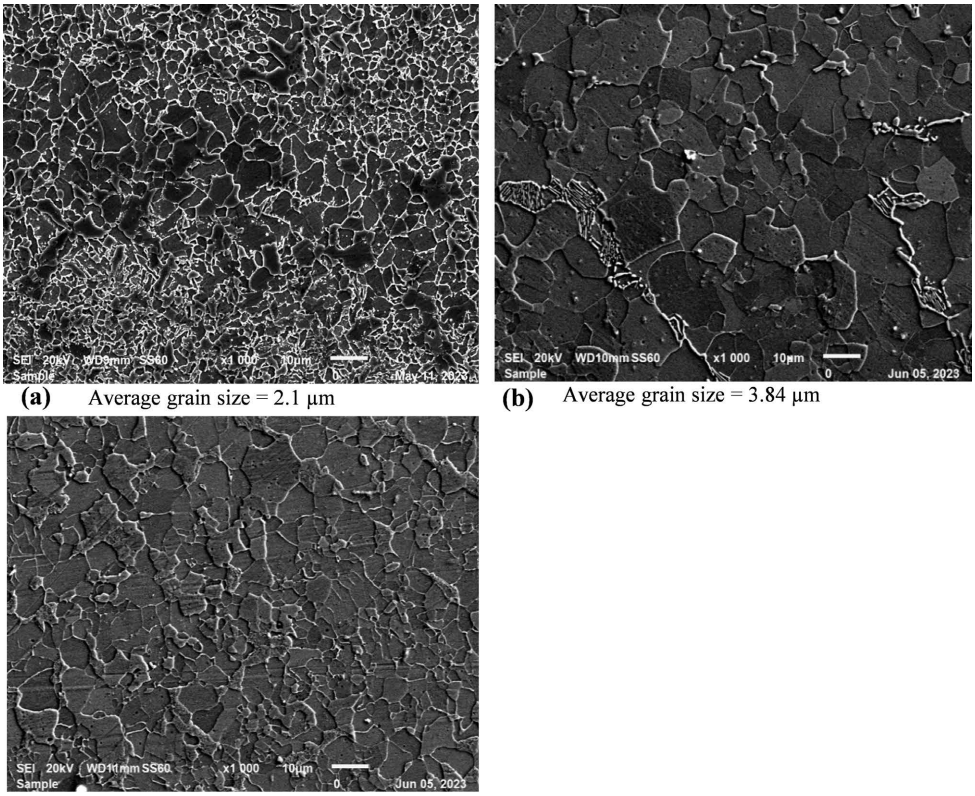

Figure 9. Representative SEM images of AISI 1025 (a) As-built microstructure; (b) Annealed microstructure; (c) Normalized microstructure.

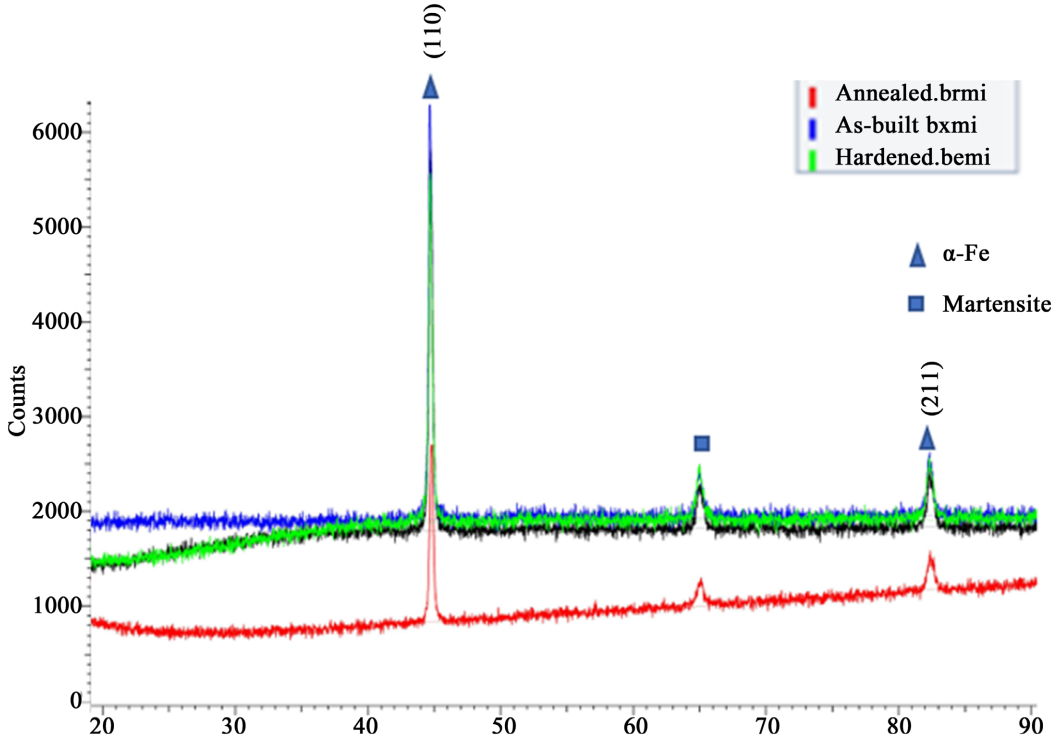

Figure 10. XRD patterns of as-built and heat treated AISI 1025.

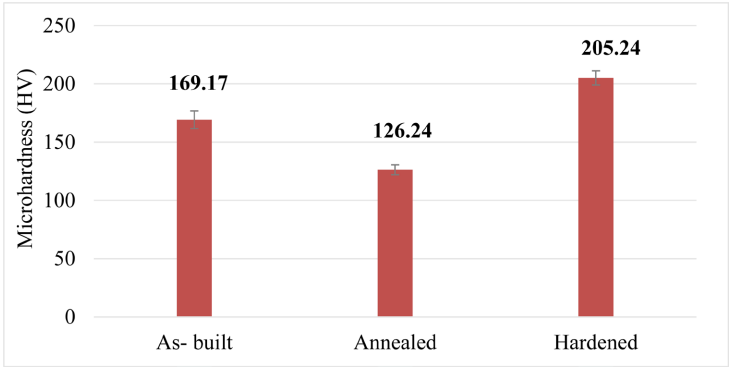

Figure 11. Microhardness in as-built, annealed, normalized and hardened samples.

into martensite. In steels, due to recrystallization and formation of martensite, a hard and brittle phase, which is known to increase strength and hardness but also induce significant residual stresses as Aversa *et al.* [28] also reported. High hardness of 205.21 ± 13.2 HV was recorded after quenching, which was related to rapid martensitic transformation [8].

4. Conclusion

This study has analyzed the impact of heat treatment on residual stress and microhardness of LENS Manufactured AISI 1025 steel. The results provide insights into the relationship between heat treatment conditions and residual stress development, highlighting the potential for utilizing heat treatment to achieve desired material properties. Annealing at a stress relaxation temperature of 850˚C resulted in grain enlargement and a 25.38% reduction in hardness, with a reduction of residual stresses to compressive of −3 MPa. On the other hand, the quenching process revealed a martensitic phase, leading to an improvement in hardness of approximately 22%, while recording high magnitudes of residual stresses of 425 MPa. Considering the results, annealing at a stress relaxation temperature of 850˚C appeared more suitable for AISI 1025 in reduction of residual stress in tool and die applications compared to the quenching process. The quenching process, with its high thermal stresses, may lead to early failure due to thermal stress-induced issues. The findings illustrate the importance of utilizing cooling rates in minimizing residual stress, thereby improving the mechanical performance and reliability of AISI 1025 steel components.

Acknowledgements

The authors appreciate Mr. Arthur Nana's assistance in operating and providing guidance on the laser system at CSIR. The work was supported by the Education for Laser-Based Manufacturing Consortium under the European Commission, project number 614655-MOBAF-2019-1-1.

Conflicts of Interest

The authors declare no conflicts of interest regarding the publication of this paper.

References

[1] Tlotleng, M. (2018) Microstructural Properties of Heat-Treated LENS *in Situ* Additively Manufactured Titanium Aluminide. *Journal of Materials Engineering and Performance*, **28**, 701-708. https://doi.org/10.1007/s11665-018-3789-5

[2] Wang, L., Felicelli, S.D. and Pratt, P. (2008) Residual Stresses in Lens-Deposited AISI 410 Stainless Steel Plates. *Materials Science and Engineering*: *A*, **496**, 234-241. https://doi.org/10.1016/j.msea.2008.05.044

[3] Bastola, N., Jahan, M.P., Rangasamy, N. and Rakurty, C.S. (2023) A Review of the Residual Stress Generation in Metal Additive Manufacturing: Analysis of Cause, Measurement, Effects, and Prevention. *Micromachines*, **14**, Article 1480. https://doi.org/10.3390/mi14071480

[4] Lu, X., Chiumenti, M., Cervera, M., Li, J., Lin, X., Ma, L., *et al.* (2021) Substrate Design to Minimize Residual Stresses in Directed Energy Deposition AM Processes. *Materials & Design*, **202**, Article IS: 109525. https://doi.org/10.1016/j.matdes.2021.109525

[5] Mugwagwa, L., Yadroitsev, I. and Matope, S. (2019) Effect of Process Parameters on Residual Stresses, Distortions, and Porosity in Selective Laser Melting of Maraging Steel 300. *Metals*, **9**, Article 1042. https://doi.org/10.3390/met9101042

[6] Zhang, X., McMurtrey, M.D., Wang, L., O'Brien, R.C., Shiau, C., Wang, Y., *et al.* (2020) Evolution of Microstructure, Residual Stress, and Tensile Properties of Additively Manufactured Stainless Steel under Heat Treatments. *JOM*, **72**, 4167-4177. https://doi.org/10.1007/s11837-020-04433-9

[7] Syed, A.K., Ahmad, B., Guo, H., Machry, T., Eatock, D., Meyer, J., *et al.* (2019) An Experimental Study of Residual Stress and Direction-Dependence of Fatigue Crack Growth Behaviour in As-Built and Stress-Relieved Selective-Laser-Melted Ti6Al4V. *Materials Science and Engineering*: *A*, **755**, 246-257. https://doi.org/10.1016/j.msea.2019.04.023

[8] Samuel, A. and Prabhu, K.N. (2022) Residual Stress and Distortion during Quench Hardening of Steels: A Review. *Journal of Materials Engineering and Performance*, **31**, 5161-5188. https://doi.org/10.1007/s11665-022-06667-x

[9] Kik, T., Moravec, J. and Novakova, I. (2017) New Method of Processing Heat Treatment Experiments with Numerical Simulation Support. *IOP Conference Series*: *Materials Science and Engineering*, **227**, Article ID: 012069. https://doi.org/10.1088/1757-899x/227/1/012069

[10] Louhichi, M.A., Poulachon, G., Lorong, P., Outeiro, J. and Monteiro, E. (2022) Experimental and Simulative Determination of Residual Stress during Heat Treatment of 7075-T6 Aluminum. *Procedia CIRP*, **108**, 82-87. https://doi.org/10.1016/j.procir.2022.03.018

[11] De Baere, D., Van Cauwenbergh, P., Bayat, M., Mohanty, S., Thorborg, J., Thijs, L., *et al.* (2021) Thermo-mechanical Modelling of Stress Relief Heat Treatments after Laser-Based Powder Bed Fusion. *Additive Manufacturing*, **38**, Article ID: 101818. https://doi.org/10.1016/j.addma.2020.101818

[12] Atanasovska, I., Nikolić-Stanojlović, V., Dimitrijević, D., Momcilovic, D. and Eng, M. (2009) Finite Element Model for Stress Analysis and Nonlinear Contact Analysis of Helical Gears. *Scientific Technical Review*, **59**, 61-69.

[13] Balichakra, M., Bontha, S., Krishna, P. and Balla, V.K. (2019) Prediction and Validation of Residual Stresses Generated during Laser Metal Deposition of γ Titanium Aluminide Thin Wall Structures. *Materials Research Express*, **6**, Article ID: 106550. https://doi.org/10.1088/2053-1591/ab38ee

[14] Cardon, A., Mareau, C., Ayed, Y., Van Der Veen, S., Giraud, E. and Dal Santo, P. (2021) Heat Treatment Simulation of Ti-6Al-4V Parts Produced by Selective Laser Melting. *Additive Manufacturing*, **39**, Article ID: 101766. https://doi.org/10.1016/j.addma.2020.101766

[15] Totten, G.E. (2006) Steel Heat Treatment: Equipment and Process Design. CRC Press.

[16] Rafieazad, M., Nemani, A.V., Ghaffari, M. and Nasiri, A. (2021) On Microstructure and Mechanical Properties of a Low-Carbon Low-Alloy Steel Block Fabricated by Wire Arc Additive Manufacturing. *Journal of Materials Engineering and Performance*, **30**, 4937-4945. https://doi.org/10.1007/s11665-021-05568-9

[17] Chae, H.M. (2013) A Numerical and Experimental Study for Residual Stress Evolution in Low Alloy Steel during Laser Aided Additive Manufacturing Process. Master's Thesis, University of Michigan.

[18] Kik, T., Moravec, J. and Švec, M. (2020) Experiments and Numerical Simulations of the Annealing Temperature Influence on the Residual Stresses Level in S700MC Steel Welded Elements. *Materials*, **13**, Article 5289. https://doi.org/10.3390/ma13225289

[19] Inoue, T. (2011) Mechanics and Characteristics of Transformation Plasticity and Metallo-Thermo-Mechanical Process Simulation. *Procedia Engineering*, **10**, 3793-3798. https://doi.org/10.1016/j.proeng.2011.06.001

[20] Moghadam, M.M., Pang, E.L., Philippe, T. and Voorhees, P.W. (2016) Simulation of Phase Transformation Kinetics in Thin Films under a Constant Nucleation Rate. *Thin Solid Films*, **612**, 437-444. https://doi.org/10.1016/j.tsf.2016.06.035

[21] Li, L. (2021) Numerical and Experimental Study of Mechanical Properties for Laser Metal Deposition (LMD) Process Part. Master's Thesis, Missouri University of Science and Technology.

[22] Shao, W., Yi, M., Tang, J. and Sun, S. (2022) Prediction and Minimization of the Heat Treatment Induced Distortion in 8620H Steel Gear: Simulation and Experimental Verification. *Chinese Journal of Mechanical Engineering*, **35**, Article No. 126. https://doi.org/10.1186/s10033-022-00802-4

[23] Directorate, E. (2019) Process Specification for the Heat Treatment of Steel Alloys. National Aeronautics and Space Administration.

[24] Lu, X., Chen, C., Zhang, G., Chiumenti, M., Cervera, M., Yin, H., *et al.* (2023) Thermo-Mechanical Simulation of Annealing Heat Treatment of Ni-Based GH4099 Superalloy Made by Laser Powder Bed Fusion. *Additive Manufacturing*, **73**, Article ID: 103703. https://doi.org/10.1016/j.addma.2023.103703

[25] Mahmoud, M., Serati, M. and Williams, D. (2021) Effect of the Minor Principal Stress on Crack Initiation Stress Threshold. *IOP Conference Series: Earth and Environmental Science*, **861**, Article ID: 042013.

[26] Hang, P.T. (2021) Effects of Heat Treatment Process on Mechanical Properties of Medium Carbon Steel. *Vietnam Journal of Agricultural Sciences*, **4**, 1283-1292. https://doi.org/10.31817/vjas.2021.4.4.07

[27] Rahman, S.M.M., Karim, K.E. and Simanto, M.H.S. (2016) Effect of Heat Treatment on Low Carbon Steel: An Experimental Investigation. *Applied Mechanics and Materials*, **860**, 7-12. https://doi.org/10.4028/www.scientific.net/amm.860.7

[28] Aversa, A., Piscopo, G., Salmi, A. and Lombardi, M. (2020) Effect of Heat Treatments on Residual Stress and Properties of AISI 316L Steel Processed by Directed Energy Deposition. *Journal of Materials Engineering and Performance*, **29**, 6002-6013. https://doi.org/10.1007/s11665-020-05061-9